Electronic Supplementary Information for

Photoinduced Ion-Redistribution in $CH_3NH_3PbI_3$ Perovskite Solar Cells

Masatoshi Yanagida, * Yasuhiro Shirai, Dhruba B. Khadka, and Kenjiro Miyano *

Centre for Green Research on Energy and Environmental Materials, National Institute for Materials Science (NIMS) 1-1 Namiki, Tsukuba, Ibaraki 305-0044, Japan.

1. Transmittance Spectrum of the Device

(a)

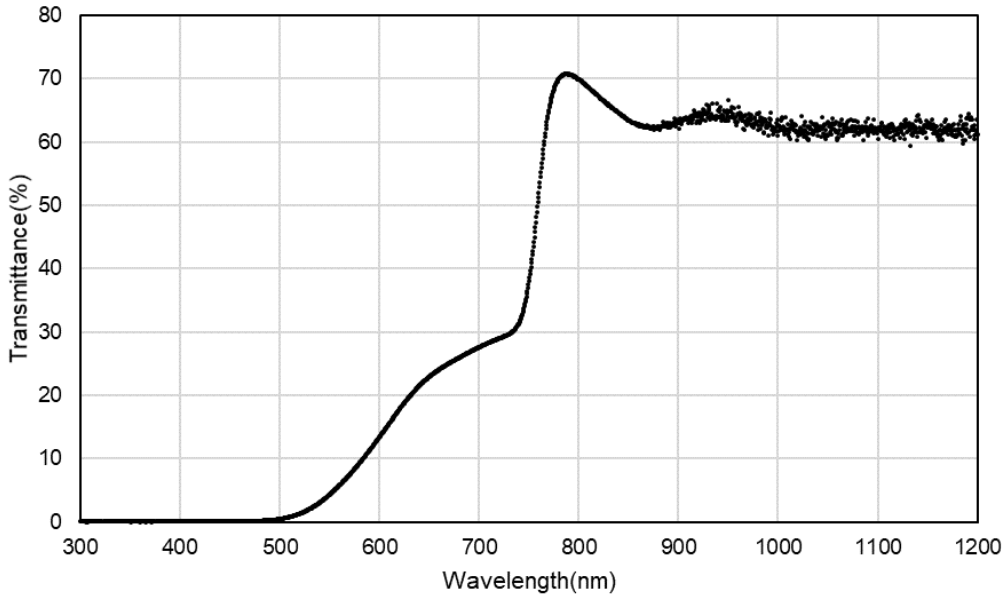

(b)

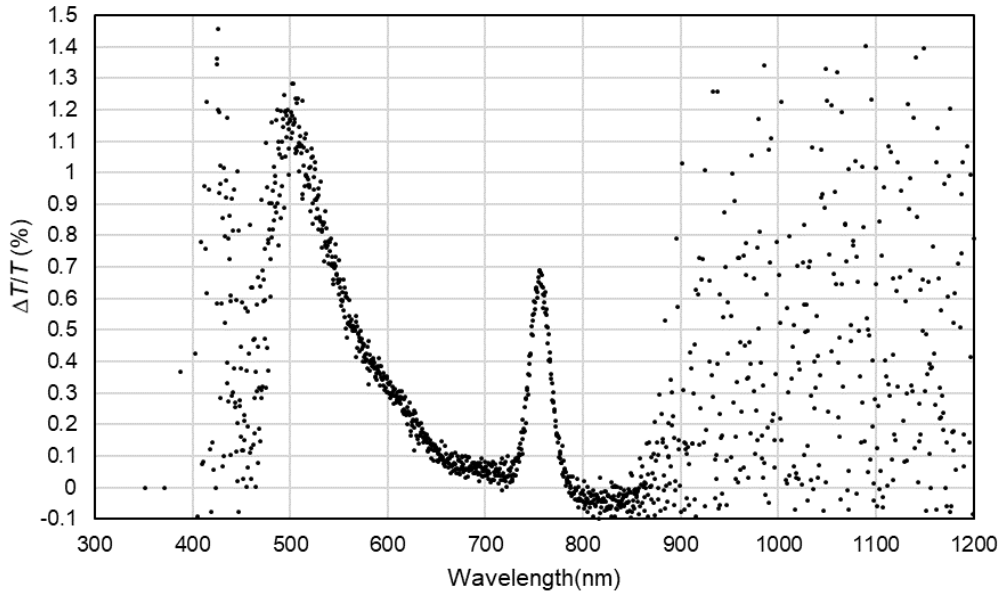

Figure S1 (a) Transmittance spectrum of the perovskite solar cell. (b) Differential spectrum of (a). The *ΔT/T* values was calculated when transmission spectrum is shifted by 0.2 nm to higher energy (blue shift).

2. Enlarged Cole-Cole plots at Various Probe Wavelength

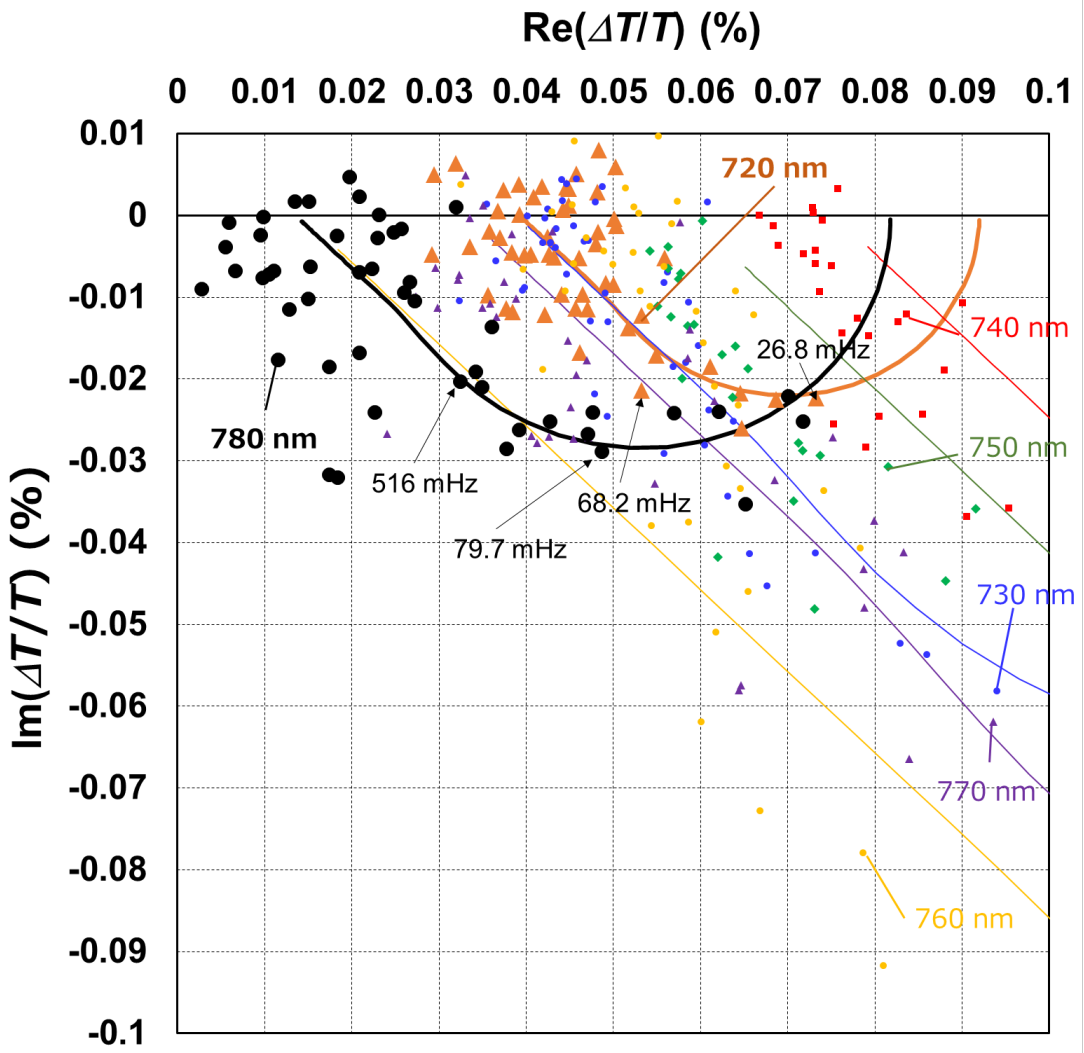

Figure S2 Enlarged Cole-Cole of *ΔT/T* at various probe wavelength. The higher frequency part (below 0.1% of Re (Δ*T*/*T*) and Im (Δ*T*/*T*)) of Fig.2 (a) is expanded.

3. Bode plots at Various Probe Wavelength

(a)

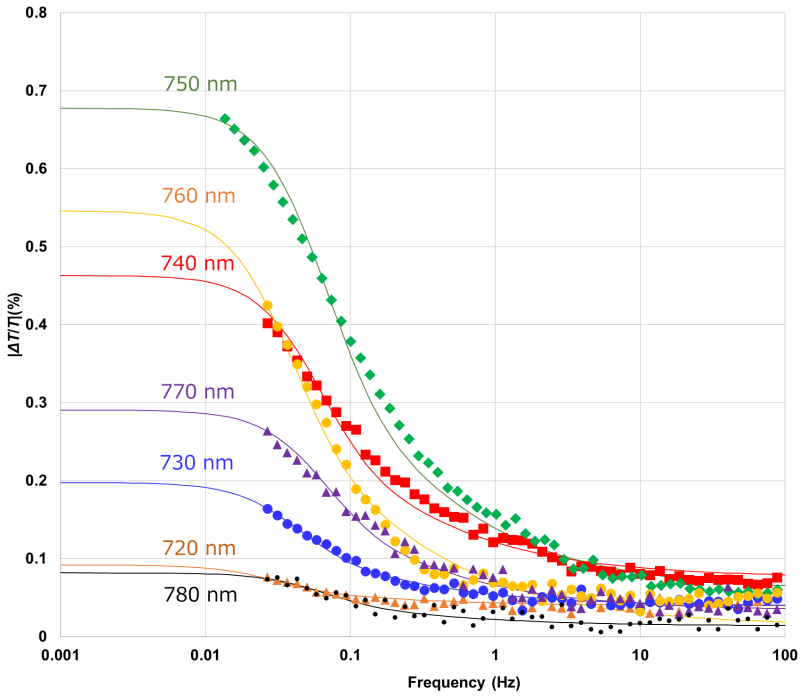

(b)

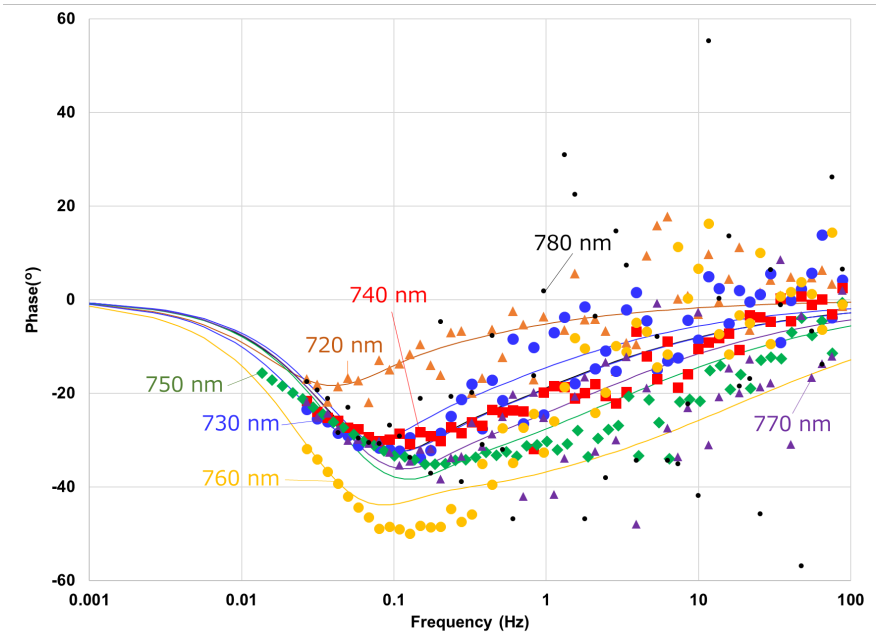

Figure S3 Bode plots of PAS results at various probe wavelength. The back lines are fitting results. (a) $|\Delta T/T|$ vs. frequency. (b) Phase vs. frequency.

4. Numerical Simulation of the Ion Distribution

4.1 General description

We interpreted the photoinduced phenomena in terms of the bandgap shift induced by the ion redistribution driven by the accumulation of photoinduced free carriers. All the charged species, photoinduced electrons and holes and mobile ions and vacancies thereof interact through the Coulombic interaction. They collectively form the electrostatic potential, ϕ, in the form of $\Delta\phi \sim -q(p-n-A+V_A)$, where q is the elementary charge and p, n, A, and V_A, are the local densities of holes, electrons, anions, and vacancies thereof, respectively. Note that we assume that the mobile ion is anion. The notable feature of a perovskite diode is that because A is extremely large, it (together with V_A) is redistributed and shields most of the bulk in a steady state. Therefore, the charge neutrality must be maintained in the bulk. This has the following consequence. Let us assume that there is a large disparity in the photoinduced carrier type, e.g., $n \gg p$. Then, a stronger illumination results in the increased n and hence reduced A, to satisfy the charge neutrality. This is the origin of the photoinduced bandgap shift. The opposite, $p \gg n$, does not result in the noticeable increase in A because of the drift force for anions toward ETL interface. There is asymmetry in the drift-diffusion characteristics.[21] In order to highlight this point, we

chose the parameter set shown in Table S1 in our numerical simulation, which is somewhat unusual but we believe it is most illustrative. We will discuss about a more realistic example in the end.

4.2 Simulation

We used a commercial numerical solver, SETFOS 5.0, for the calculation. The simulation consists of 1D coupled drift-diffusion equations for free carriers (electrons and holes) and for ions (mobile ions - we assume anions - and the vacancies thereof). The electron-ion coupling is through the Coulombic interaction only: electrons and holes can recombine, and anions and vacancies can also recombine. In the equilibrium, A and V_A are distributed uniformly and equal (denoted as A_0 and V_{A0}, respectively) creating no ion-induced potential ($-A_0+V_{A0} = 0$). Under external perturbation, A redistributes to counteract the perturbation leaving V_A behind. For example, the built-in potential created by the contacts attracts A to the ETL and V_A is accumulated at the HTL. No limit is set to A (meaning that it can be considerably larger than A_0) while V_{A0} cannot be less than 0. Therefore, the double layer at the ETL is very thin (a few nm for A_0~10^{18} cm^{-3}) and acts as a reservoir for A while the double layer at the HTL is much thicker.

In order to show the essence of the scenario described in 4.1 General description, we

chose a set of parameters shown in Table S1 in the simulation. They are designed to achieve $n \gg p$ and some spatial variation in n under illumination. Let us consider the short-circuit case, which corresponds to the experimental condition shown in Fig. 2 in the main text. In the dark, the distribution of all the charged species is flat in the bulk of the perovskite (beyond some distance away from the interfaces) and the potential is also flat. Under light illumination, n is generated everywhere in the perovskite but there is the density distribution due to the smallness of the diffusion constant for electrons. This is shown in Fig. S4 (a). The electron density distribution is counteracted by the oppositely distributed anion shown in Fig. 3 in the main text. The sum of n and A indeed recovers the flat distribution of total negative charges as shown in Fig. S4 (b).

Table S1 Parameters of the numerical simulator.

ETL LUMO (ohmic contact) (eV)		3.85	
HTL HOMO (ohmic contact) (eV)		5.38	
Perovskite	CBM*(eV)	3.82	
	VBM*(eV)	5.44	
Electron Mobility ($cm^2V^{-1}s^{-1}$)		0.01	1
Hole mobility ($cm^2V^{-1}s^{-1}$)		1	0.01
Mobile ion density (cm^{-3})		Anion 10^{18}	Cation 10^{18}
Illumination of 520 nm ($mWcm^{-2}$)		0 – 100	

* CBM is the conduction band minimum and VBM is the valence band maximum, respectively.

(a)

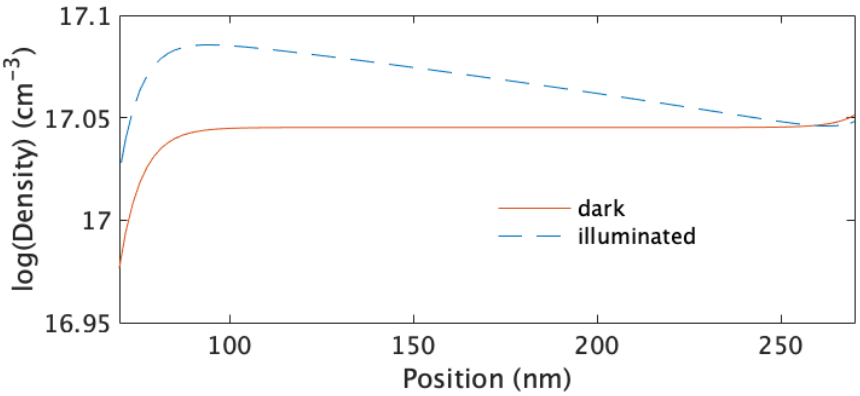

(b)

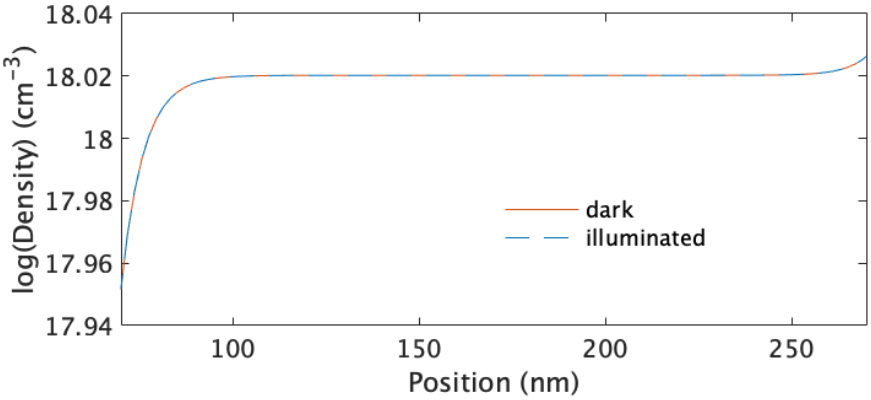

(c)

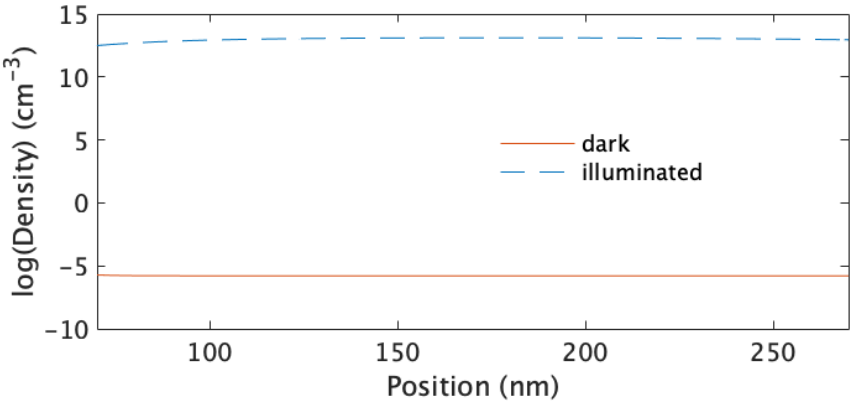

Figure S4 Charge density distribution in the dark and under the illumination. (a) electron (n), (b) electron + anion ($n + A$), and (c) hole (p). Two curves for $n + A$ are on top of each other.

It is to be noted that the bulk is automatically "n-doped" because of the sign of the mobile ion and the ohmic contacts. That this is not because of the relative position of energy levels is confirmed as follows. Without changing the energy levels of the model but simply by interchanging the role of electron and anion with that of hole and cation as listed in Table S1, we obtain the photoinduced cation density shift as shown in Fig. S5. It is clear that the mobile ion responds to the photo carrier concentration of the same sign.

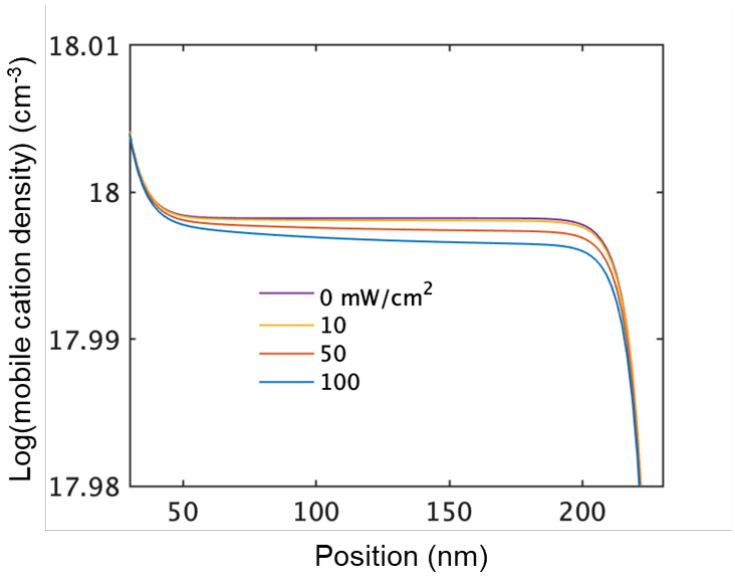

Figure S5 Simulation when cation is mobile. HTL/perovskite and perovskite/ETL interfaces are located at 0 and 300 nm, respectively.

It may seem that the choice of the parameters in Table S1 is unusual and that is the cause of the phenomenon. One can choose a more realistic model with parameters listed in Table S2, where both contacts are doped semiconductors and are 50 nm thick. A 2 nm thick blocking layer on the HTL is introduced to achieve $n-p$ asymmetry. The perovskite layer

is 400 nm thick (occupying 52 nm – 452 nm in position) and cation is mobile with the density of 10^{17} cm^{-3}. The distribution of electrons and holes is shown in Fig. S6 (a). In the dark, n~p~0 as is expected. The enhanced increase in the photoinduced holes produce corresponding depression in the cation in the bulk (Fig. S6 (b)).

(a)

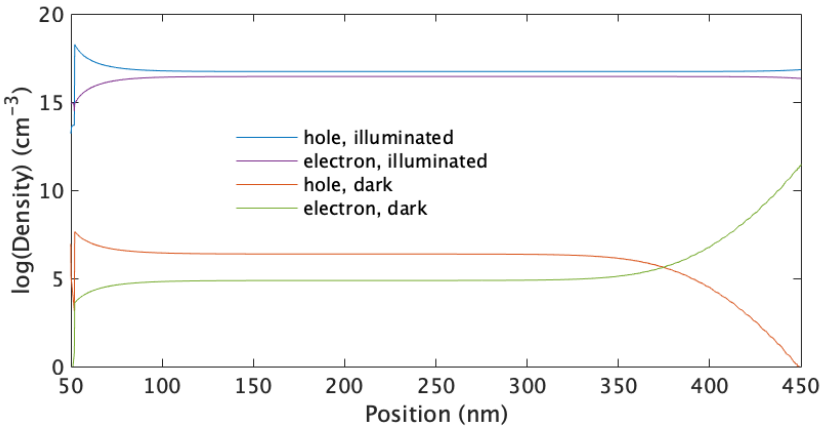

(b)

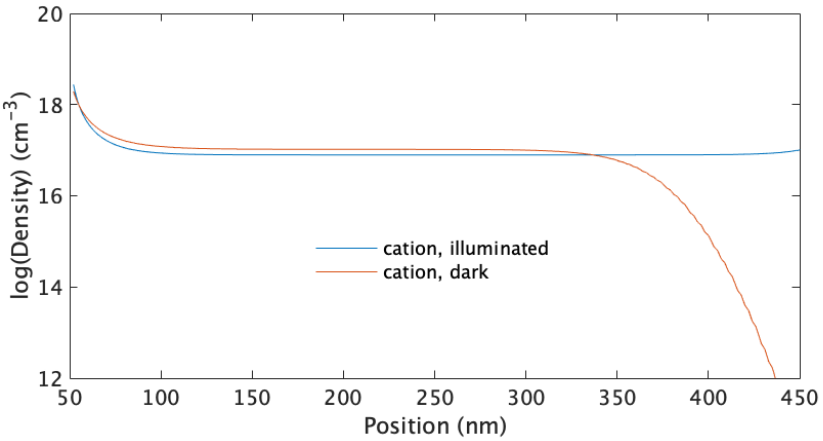

Figure S6 Charge distribution in the dark and under the illumination. (a) electrons and holes, (b) cations.

Table S2 Parameters for a more realistic model.

ITO electrode	work function 5.2 eV
HTL 50 nm	gap: 5.38 – 3.59 eV, acceptor doped 10^{18} cm^{-3}
blocking layer 2 nm	gap: 5.78 – 3.59 eV, non-doped
perovskite 400 nm	gap: 5.44 – 3.82 eV, mobile cation 10^{17} cm^{-3}
ETL 50 nm	gap: 5.77 – 3.85 eV, donor doped 10^{18} cm^{-3}
Ag electrode	work function 4.1 eV

Although, it is not practical to perform exhaustive calculations for realistic parameter sets, we believe that the free carrier – mobile ion interaction is well supported.

5. Justification of using Eqn (2)

It is numerically easier to simulate the transient response of mobile ion upon the application of a step function light rather than calculate its response to a sinusoidal light modulation over a wide frequency range. (The contrary is true for experiments.) Therefore, we calculated the response of a system that shows Warburg spectrum to a step function input, which was then compared with the above numerical simulation.

Following the standard procedure,[55] we calculated a response of a Warburg system to a step function input as follows;

$$S(t) = \int_0^\infty Re\left(\frac{W(\sqrt{i\omega})}{i\omega}\right)\cos(t\omega)\,d\omega. \qquad \text{(S1)}$$

where t is time (s).

We also simulated the response of a perovskite device upon the input of a step function illumination, $Q(t)$, for which we chose the ion density value at the center of the device. We tried to "imitate" $Q(t)$ by adjusting a set of scaling parameters for the limiting values for $t \to 0$ and $t \to \infty$ such that $Q(t) \approx a + b \cdot S(t)$: a and b are adjustable parameters. The results are shown in Fig. 4 in the main text. Here, the numerical simulations were done for three ion mobilities, $\mu = 10^{-8}, 10^{-7}$, and 10^{-6} $cm^2V^{-1}s^{-1}$. The shapes of $Q(t)$

for different μ are similar when presented in log(t) scale and shifted by one decade from each other, as is expected. The Fourier transform, eqn (S1) is related to the real Warburg element by the transformation $\omega \rightarrow Dt/L^2$. In Fig. 4, the normalized form ($D/L^2 = 1$) is shown in circles. If we assume $D = 1 \times 10^{-10}\,\mathrm{cm^2 s^{-1}}$ and L = 300 nm, the Fourier transform shown in crosses results. The Fourier transform of the Warburg element is remarkably similar to the numerical simulations of the transient behavior.

The inflection point of the Fourier transformed curve in crosses is located around 3 s. This means that the peak of the Cole-Cole plot occurs around 100 mHz, recovering our results in Fig. 2(a) as should be the case. From the numerical simulation, the transient curve with an inflection point around 3 s would imply the mobility of $\mu \approx 3 \times 10^{-10}\,\mathrm{cm^2 V^{-1} s^{-1}}$ bringing $D \approx 10^{-11}\,\mathrm{cm^2 s^{-1}}$ at room temperature. This is a slight underestimation, which could be due to overestimation of the mobile ion density in the numerical simulation. However, we believe that the results obtained through different physical considerations are reasonably consistent between each other.

6. Bode Plots at Various Light Intensity

(a)

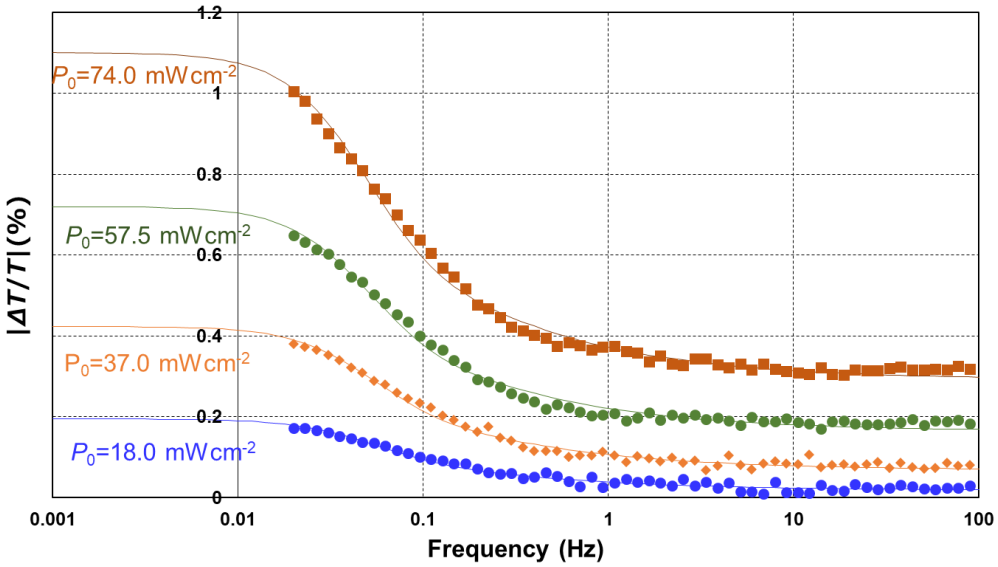

(b)

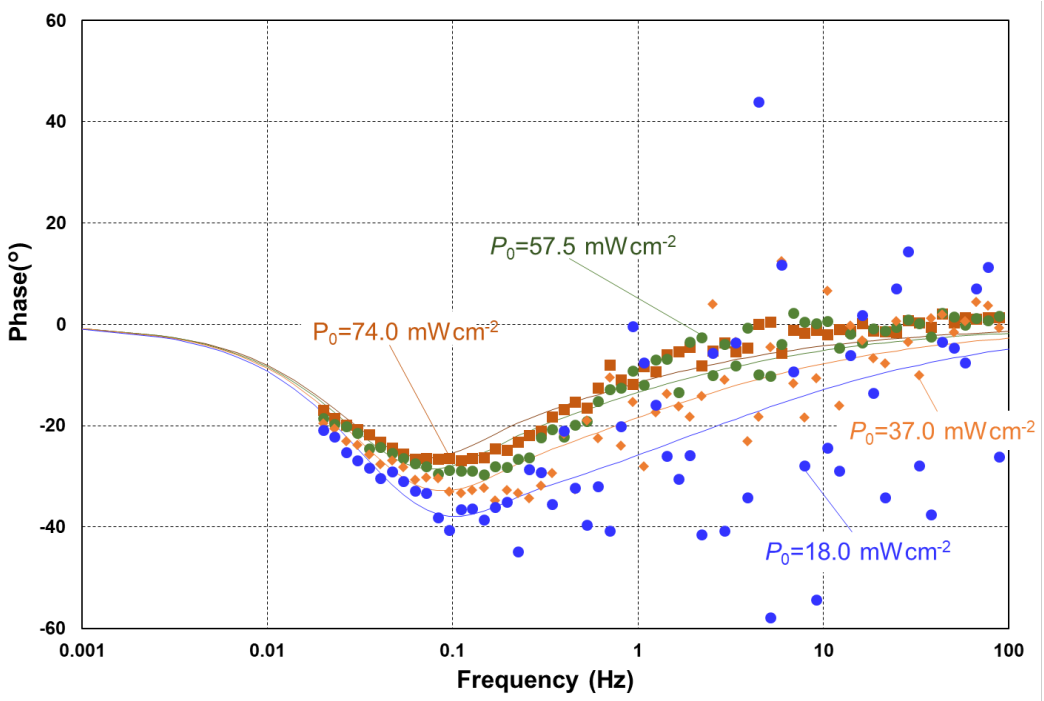

Figure S7 Bode plots of PAS results at various light intensity (P_0). The lines are fitting results. (a) $|\Delta T/T|$ vs. frequency. (b) Phase vs. frequency.

Table S3 Fitting results of Cole-Cole plots in Fig. 5(a) and S7.

Light power(P_0) ($mWcm^{-2}$)	J_{SC} a) ($mAcm^{-2}$)	D (10^{-11} cm^2s^{-1})	$\{\Delta T(0)-\Delta T(\infty)\}/T$ (%)
74.0	26.4	6.1	0.81
57.5	20.5	6.2	0.56
37.0	13.2	6.5	0.36
18.0	6.4	6.6	0.18

a) The J_{SC} values are the maximum photocurrent density under the modulated illumination.

7. Bode Plots and Numerical Simulation for Applied Bias Dependence

(a)

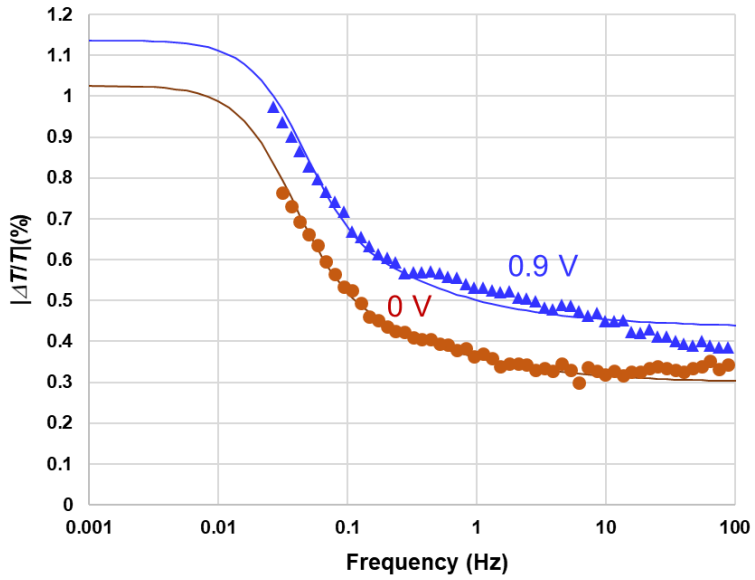

(b)

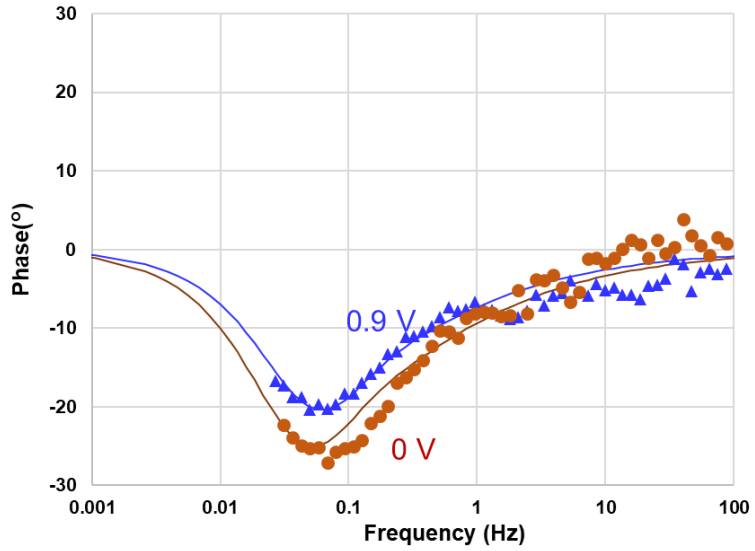

Figure S8 Bode plots of PAS results at the applied bias voltage of 0 V and 0.9 V, respectively. The maximum photocurrent density at 0 V and 0.9 V was 21.5 $mAcm^{-2}$ and 2.6 $mAcm^{-2}$, respectively under modulated illumination. The black lines are fitting results. (a) Bode plot of $|\Delta T/T|$ vs. frequency. (b) Phase vs. frequency.

The charge imbalance persists under applied bias voltage. An example is shown in Fig. 6, under an applied voltage $V = 0.9$ V.

Table S4 Fitting results of Cole-Cole plots in Fig. 6 and S8.

Bias (V)	J(mAcm^{-2})	D (10^{-11} cm^{2}s^{-1})	$\{\Delta T(0)$-$\Delta T(\infty)\}$/T
0.0	21.5	4.7	0.73
0.9	2.6	6.0	0.70

The results of numerical simulations under different light intensity and bias voltage are summarized in Fig. S9, in which the ion density deficiency relative to the equilibrium value of 10^{18} cm^{-3} at the center of the device position = 150 nm is plotted. The qualitative characteristics of our observation are well reproduced: the linear dependence on the light intensity and the slight reduction under applied bias voltage.

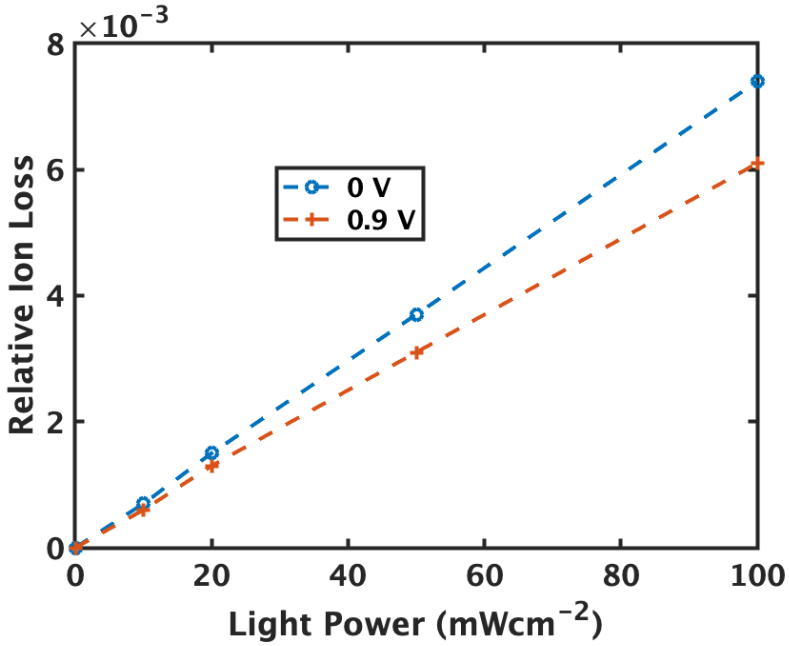

Figure S9 The relative ion deficiency at the center of the device.

8. Reflection Measurement

In the present study, the device design is restricted because we should maintain a reasonable transmittance through the device. If we use the reflectance, we can cover a wider design parameter space. Because the transmission and reflection are related, we should be able to extract the same information. An example is shown in Fig. S10, where the transmission data used in the main text and the reflection data for another device are plotted. The vertical scales are adjusted to reflect the different optical processes. It is clear that the overall characteristics are similar but there is a slight shift in the frequency, suggesting that there is a slight thickness difference.

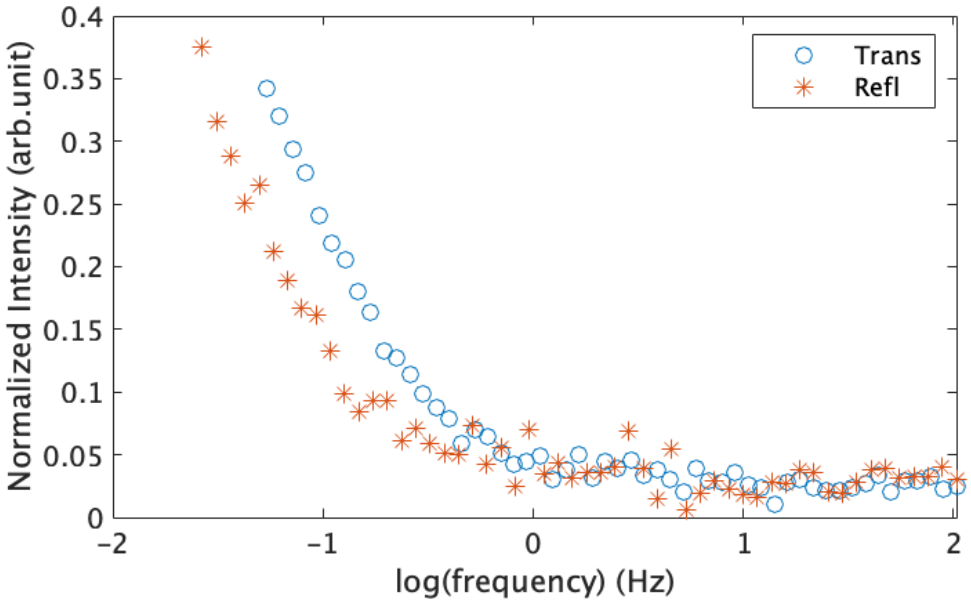

Figure S10 Frequency dependence of the signal amplitude of a device obtained by transmission measurement and that of another device by the reflection measurement. Slight frequency shift suggests that the slight thickness difference, although they are fabricated nominally by the same method.